Recent Results of the Chinese CMONOC GNSS Network

Article · May 2017

CITATIONS
0

READS
14

6 authors, including:

Junping Chen
Chinese Academy of Sciences
71 PUBLICATIONS **451** CITATIONS
SEE PROFILE

Sainan Yang
Chinese Academy of Sciences
17 PUBLICATIONS **14** CITATIONS
SEE PROFILE

Jungang Wang
Tongji University
11 PUBLICATIONS **14** CITATIONS
SEE PROFILE

Yize Zhang
Tongji University
32 PUBLICATIONS **68** CITATIONS
SEE PROFILE

Recent Results of the Chinese CMONOC GNSS Network

Junping Chen[1,2], Sainan Yang[1,2], Weijie Tan[1,2], Jungang Wang[3], Qian Chen[1,2], Yize Zhang[1]
1 Shanghai Astronomical Observatory, Shanghai 200030,China
2. School of Astronomy and Space Science, University of Chinese Academy of Sciences, Beijing 100049, China
3 Technical University of Berlin, 10623 Berlin, Germany

BIOGRAPHIES

Prof. Junping Chen is the head of the GNSS data analysis group at Shanghai Astronomical Observatory (SHAO). He received his Ph.D. in Satellite Geodesy from Tongji University in 2007. From June 2006 to April 2011, he worked at the GFZ in Potsdam as research scientist. Since 2011, he has been supported by the "one hundred talents" program of the Chinese Academy of Sciences and works as the leader of the GNSS Analysis Center at the Shanghai Astronomical Observatory (SHAO). His research interests inlcude multi-GNSS data analysis and GNSS augmentation systems.

Sainan Yang is a Ph.D. student at SHAO. Her recent research interests include BDS augmentation and ionosphere modeling.

Weijie Tan is a Ph.D. student at SHAO. Her recent research interests include GNSS tectonics, geophysical signal analysis and modelling of GNSS time series.

Jungang Wang is a Ph.D. student at the Technical University of Berlin in Germany. He worked as a part-time research associate at SHAO from 2014-2016.

Qian Chen is a Ph.D. student in SHAO. Her recent research interests include GNSS augmentation and precise orbit determination.

Yize Zhang is Ph.D. in the College of Surveying and Geo-informatics Engineering at Tongji University. He works as a part-time research associate at SHAO. His recent research interests include precise point positioning (PPP) and real-time clock estimation.

ABSTRACT

Crustal Movement Observation Network Of China (CMONOC) is a fundamental facility, which has a wide range of applications in diverse areas with high precision and high spatial resolution. Consisting of 260 continuous sites and more than 2,000 campaign sites, CMONOC GNSS network contributes to the meteorology, plate tectonics earthquake monitoring, etc. As one of the data centers of the CMONOC network, Shanghai Astronomical Observatory(SHAO) developed the CMONOC GNSS data processing facilities and provides precise products supporting various CMONOC applications. Our routine GNSS data analysis is performed using the data of the CMONOC network as well as the international GNSS service (IGS) network. In this paper, we present the latest results and findings of the routine analysis, including: (1) regional horizontal and vertical velocity field of China mainland; (2) the refined emperical troposperic zenith delay model CZTDw over China mainland, which shows higher accuracy than other published models; and (3) earthquake co-seismic monitoring and optimum estimation of lithosphere viscosity for the post-seimic deformation modeling.

INTRODUCTION

Crustal Movement Observation Network Of China (CMONOC) is in operation since 1999. It is a fundamental facility, which has wide range of applications in diverse areas with high precision and high spatial resolution. It consists of 260 GNSS continuous sites, several Very Long Baseline Radio Interferometry (VLBI) sites and Satellite Ranging (SLR) and precise leveling and gravity sites. Observation data of CMONOC has contributed to the field of the GNSS meteorology [1], plate tectonics and earthquake

monitoring [2].

As one of the data centers of the CMONOC, SHAO has operated the routine GNSS data analysis since June 2011 [3]. Data analysis implements similar strategies as it used in our IGS routine data analysis [4]. In the CMONOC routine analysis, we combine the observations from the IGS and CMONOC network, and all solutions are aligned to the latest release of international terrestrial reference frame (ITRF). In our routine analysis, precise orbits, clocks, troposphere and coordinates, etc., are derived on a daily basis [5]. Based on these precise products, we present for the first time the following new results: (1)regional horizontal and vertical velocity field for China mainland; (2) the refined emperical troposperic zenith delay model CZTDw over China mainlad, which shows higher accuracy than other published models; and (3) earthquake co-seismic monitoring and optimum estimation of lithosphere viscosity for the post-seimic deformation modeling.

VELOCITY FIELD OF THE CMONOC GNSS SITES

SHAO has operated the routine GPS data analysis since June 2011, where around 70 globally distributed IGS stations and 260 CMONOC stations are included in daily solutions. The GPS carrier phase data from all the stations have been processed using the iGPOS (integrated Geodetic Platform Of SHAO) Software. Processing models and strategies are similar as used in our IGS *zero-difference*-based routine data analysis[4]. Independent baselines are selected according to maximum common observation strategy. The double-differenced ambiguities are resolved using the rounding strategy, and the fixed double ambiguities are then used as constraints in *zero-difference-based normal equations.* The station coordinates are estimated together with troposphere parameters, where 24 Zenith path delays per day per station with one set of horizontal gradient parameters per day per station are estimated. Together with station coordinates, satellite orbits/clocks and weekly Earth rotation parameters are estimated.

Each daily solution is aligned to the latest ITRF reference frame by applying minimum constraint on the helmert transformation parameters. The daily solutions are combined using the QOCA (Quasi-observation Combination Analysis) software to derived velocity field (Figure 1, 2).

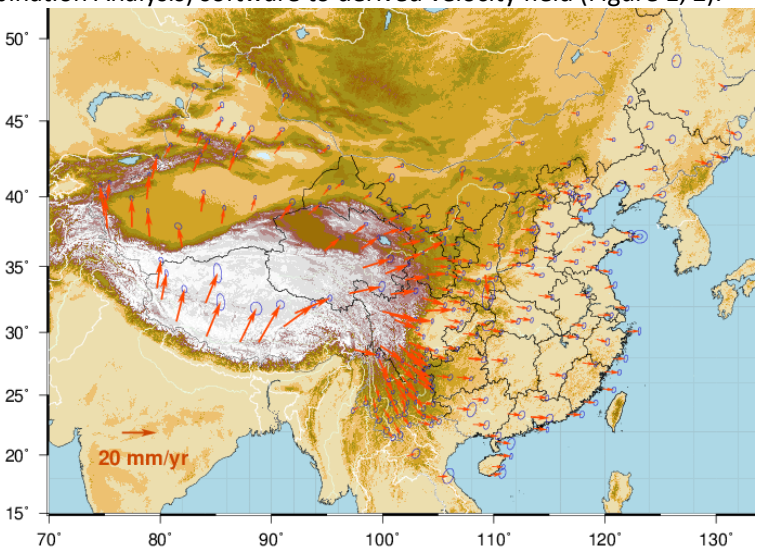

Figure 1 The horizontal velocity field estimated by SHAO based on the CMONOC observations . The red arrows represent the slip rate for each site. The ellipses represent the 95% confidence level.

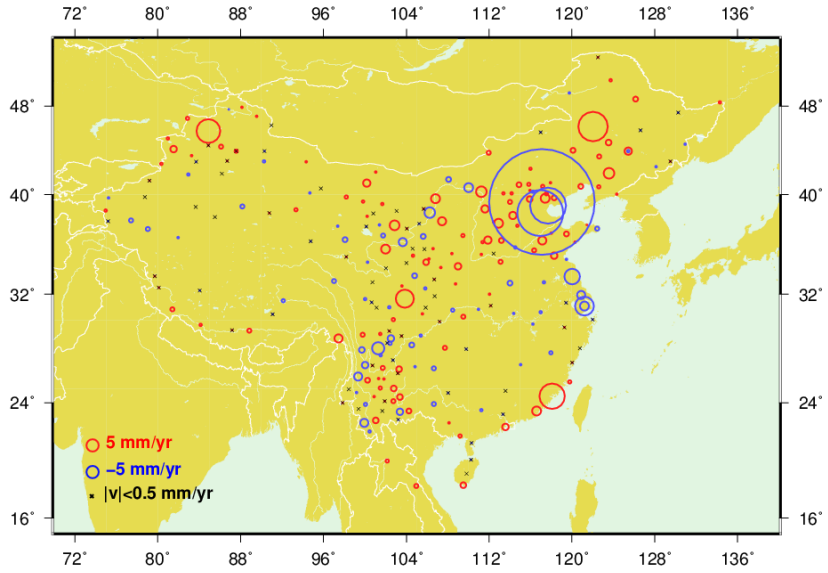

Figure 2 The vertical velocity field estimated by SHAO based on the CMONOC sites . The red circles represent the sites move upward; the blue circles mean the sites move downward. For the black crosses, the sites' slip velocities are less than 0.5 mm yr^{-1}.

REFINED TROPOSPHERIC ZENITH DELAY MODEL BASED ON CMONOC NETWORK

Besides coordinate time series, we derive also zenith tropospheric delay (ZTD) time series for each station at the sampling of one hour in our routine GNSS analysis. For the estimation of tropospheric zenith delay, the dry part is calculated using the GPT model together with Global Mapping Function (GMF). The accuracy of estimated tropospheric zenith delay from SHAO (abbreviated as SHA ZTD) is evaluated by comparison with the IGS tropospheric product (abbreviated as IGS ZTD), which has an accuracy of ~2mm. Comparison between IGS ZTD and SHA ZTD is performed. The average bias and the root mean square (RMS) of ZTDs of these sites are calculated as follows:

$$RMS = \sqrt{\frac{1}{N}\sum_{i=1}^{N}\left(ZTD_i^{IGS} - ZTD_i^{SHA}\right)^2}$$
$$BIAS = \frac{1}{N}\sum_{i=1}^{N}\left(ZTD_i^{IGS} - ZTD_i^{SHA}\right) \quad (1)$$

Where ZTD_i^{IGS} and ZTD_i^{SHA} are IGS ZTD and SHA ZTD, and N is the number of ZTDs. Table 1 shows the comparison results of the seven IGS stations in China mainland over the year 2011-2016. We see the average bias and RMS of the seven IGS stations are 0.9 mm and 2.7 mm, respectively.

Table 1 Statistics of SHA ZTD comparing to IGS ZTD

	BJFS	SHAO	CHAN	LHAZ	URUM	KUNM	TWTF	Mean
BIAS(mm)	1.2	-0.7	1.5	1.5	1.0	1.0	1.0	0.9
RMS(mm)	2.0	2.0	2.3	2.6	1.6	3.8	1.6	2.7

The following figure shows the zenith wet tropospheric delay (ZWD) of four sites locating at north east, north west, and south part of China mainland with different altitudes. Clearly, temporal variations containing annual and semi-annual signals dominate the ZWD time series. The annual term could be fitting using the following model:

$$ZWD(doy) = ZWD_0 + A_1 \cos\left(\frac{2\pi}{365.25}(doy - d_1)\right) \tag{2}$$

In Eq. (2), doy is day of the year, ZWD_0 is a constant term; A_1, d_1 are amplitude and initial phase of annual component. Taking the annual and semi-annual terms into consideration for the modelling of ZWD, we have the following model:

$$ZWD(doy) = ZWD_0 + A_1 \cos\left(\frac{2\pi}{365.25}(doy - d_1)\right) + A_2 \cos\left(\frac{4\pi}{365.25}(doy - d_2)\right) \tag{3}$$

In Eq. (3), ZWD_0, A_1, d_1 are the same as in Eq. (2), and A_2, d_2 are the amplitude and initial phase of semi-annual term.

The fitting curves of the four sites are also shown in figure 3, where we see that the fitted ZWDs using the two fitting methods show good agreement with the estimated ZWD. Fitting model based on Eq. (3) performs better than that of Eq. (2), especially in summer and winter seasons. For sites at high latitude, e.g. HLHG (47° N, 130° E, 210 m), the difference between the two models can be as big as three centimeters in summer and winter, while for sites at lower latitude, e.g., QION (19° N, 109° E, 207 m), the difference could be negligible.

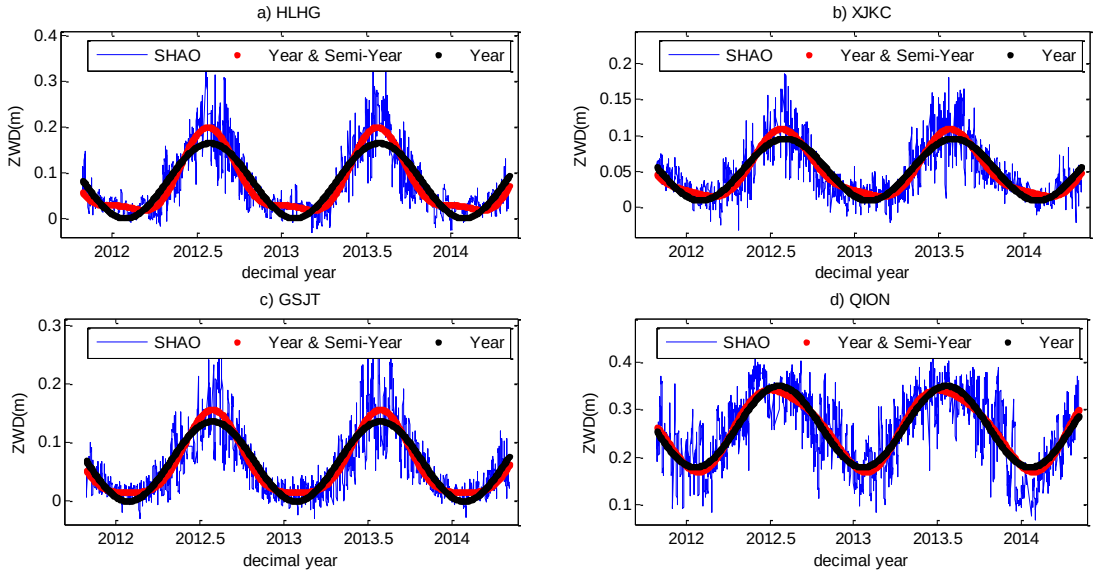

Figure 3 ZWD time series and fitting curves for stations a) HLHG (47° N, 130° E, 210 m); b) XJKC (42° N, 83° E, 1028 m); c) GSJT (37° N, 104° E, 1603 m); d) QION(19° N, 109° E, 207 m)

Based on the long periods of precise ZTD estimates of SHAO, we develop a refined regional model CZTDw. The initial form of CZTDw is defined as follows:

$$\begin{aligned} ZTD(\varphi,\phi,h,doy) &= ZHD^{GPT}(\varphi,\phi,h,doy) + ZWD(\varphi,\phi,doy) \times e^{\beta h} \\ ZWD(\varphi,\phi,doy) &= ZWD_0(\varphi,\phi) + A_1(\varphi,\phi)\cos\left(\frac{2\pi}{365.25}(doy - d_1(\varphi,\phi))\right) \\ &\quad + A_2(\varphi,\phi)\cos\left(\frac{4\pi}{365.25}(doy - d_2(\varphi,\phi))\right) \end{aligned} \tag{4}$$

where ZHD^{GPT} is the hydrostatic zenith delay derived from GPT model; (φ,ϕ,h) are the latitude, longitude, altitude of the station; (A_1, d_1) and (A_2, d_2) are the same as in Eqs. (2) and (3) but with the function of sites' latitude and longitude; e is Euler's number, ZWD_0 is ZWD at the geoidal surface, and $\beta = -0.4027 \times 10^{-3}$ is the exponential constant.

CZTDw is expressed in 2.0 by 2.5-degree latitude/longitude grid, where the gridded parameter set includes a constant term ZWD_0, annual/semi-annual amplitudes (A_1, A_2) and initial phases (d_1, d_2). The gridded CZTDw parameters at each grid are determined based on Eq. (4), where ZWDs of each CMONOC GNSS site in the grid are used as inputs.

Applying the new emperical model CZTDw, troposhperic zenith delays could be calculated for sites located inside China mainland. For the evaluation of the CZTDw model, ZTDs calculated based on the CZTDw model are compared against the precise SHA ZTDs of each CMONOC site. We seperate the evaluation as inner- and external-accuracy evaluation, where inner-accuracy is calculated based on the sites used for the determination of CZTDw, and external-accuracy is calculated based on the other stations. Table 2 shows the statistics, including the average bias and the RMS. From Table 2 we see that: 1) the mean difference between inner- and external-accuracy statistics is less than 2mm, showing similar accuracy is achieved for all grids in the CZTDw model; 2) ZTD and ZWD calculated from CZTDw have a mean RMS of 3.5 cm with 1.2 cm and 6.5 cm as minimum and maximum errors; 3) ZTD and ZWD calculated from CZTDw have a mean bias in the range of [-0.2, 0.1] cm with -2.5 cm and 2.7 cm as minimum and maximum errors; 4) ZWD shows smaller range in the distribution of RMS and bias values.

Table 2 Bias and RMS statistics of CZTDw in unit of cm, '[ ]' show the minimum and maximum value

		ZTD	ZWD
inner-accuracy	RMS	3.5 [1.4, 6.5]	3.5 [1.4,6.5]
	BIAS	-0.1 [-2.5, 2.4]	-0.2 [-2.3,1.6]
external-accuracy	RMS	3.5 [1.3, 6.5]	3.5 [1.2,6.5]
	BIAS	0.1 [-1.9, 2.7]	0.1 [-2.2,1.7]

To further evaluate CZTDw, ZTD modelling errors of EGNOS/UNB3m/GPT2 are calculated for the same time period. Figure 4 plots the ZTD RMS of each station. It is shown that CZTDw achieves the best accuracy comparing to the EGNOS/UNB3m/GPT2. For sites in most part of China, the RMS of CZTDw is smaller than 5 cm, and the maximum RMS appears in the vicinity of (30° N, 120° E).

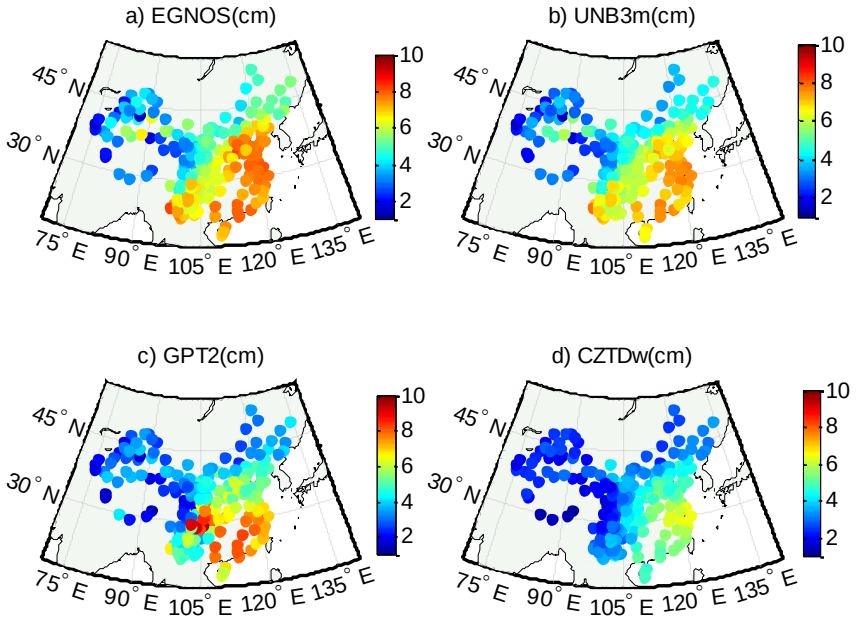

Figure 4 RMS of CZTDw comparing to EGNOS/UNB3m/GPT2 models (in cm)

EARTHQUAKE CO-SEISMIC AND POST-SEISMIC DEFORMATION MONITORING

Another application of the CMONOC GNSS network is to monitor the co-seismic and post-seismic deformation due to earthquake. Take the Xinjiang Ms6.6 earthquake on June 30, 2012 as an example. The earthquake happened at 05:07:31 (UTC 21:07:31 on June 29), and the stations XJSH (137 Km away from epicenter, sampling 1s) and XJKC (240 Km away from epicenter, sampling 1s) track the co-seismic displacement. Instantaneous velocity and co-seismic offsets are shown in the following figures for these two sites. Both the estimated instantaneous velocity and co-seismic offsets show obvious changes when the seismic waves reach these stations, where maximum amplitude of instantaneous velocity reaches 16 mm/s for XJSH and 13 mm/s for XJKC, and the maximum co-seismic offset reaches 11 mm for XJSH and 10 mm XJKC, respectively. The shaking effects continue for around 20 seconds, the stations become static and the estimated instantaneous velocity restores to white noise after that. We observe that the epoch when seismic waves arrive at the station XJSH is around 31 seconds ahead of the time it reaches XJKC. Based on the time difference, we calculate the seismic waves speed as 3.32Km/s.

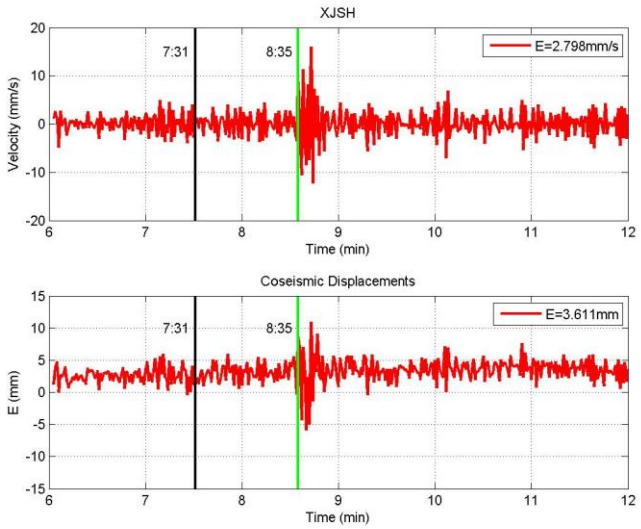

Figure 5 Velocity change and co-seismic displacement time series of station XJSH, where black line shows the earthquake epoch and green line is the approximate time that the seismic waves reach the site

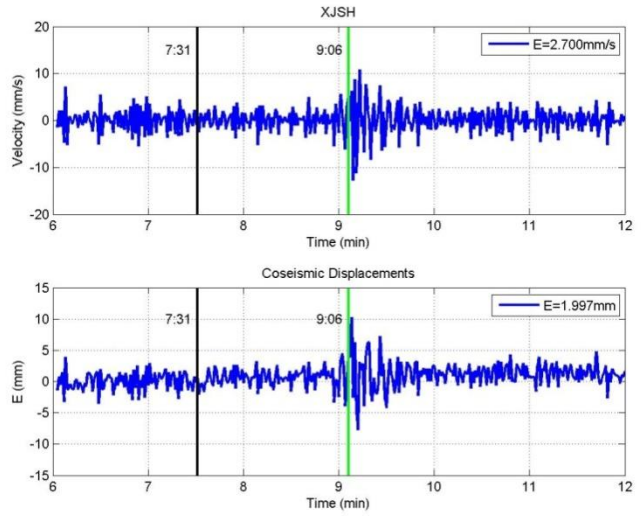

Figure 6 Velocity change and co-seismic displacement time series of station XJKC, where black line shows the earthquake epoch and green line is the approximate time that the seismic waves reach the site

Another recent result of earthquake-related research is the post-seismic deformation

monitoring. The 2001 Kokoxi earthquake-induced post-seismic deformation has been recorded by geodetic techniques. It occurred at the seismic gaps of east Kunlun Fault zone, where short-term post-seismic deformation for the Kokoxili earthquake has lasted for six months. We assess the 2001 earthquake velocity responses to the stress variation using the long period coordinate time series of station DLHA (37.4°N, 97.4°E). The horizontal coordinate components time series of DLHA is shown in figure 7, where a clear jump of -7.48 mm in east direction, and -4.7 mm in north direction due to earthquake could be observed. And the modeled velocities from GPS observations are *-0.19 mm yr^{-1}, and -0.14mm yr^{-1}* for the east and north components.

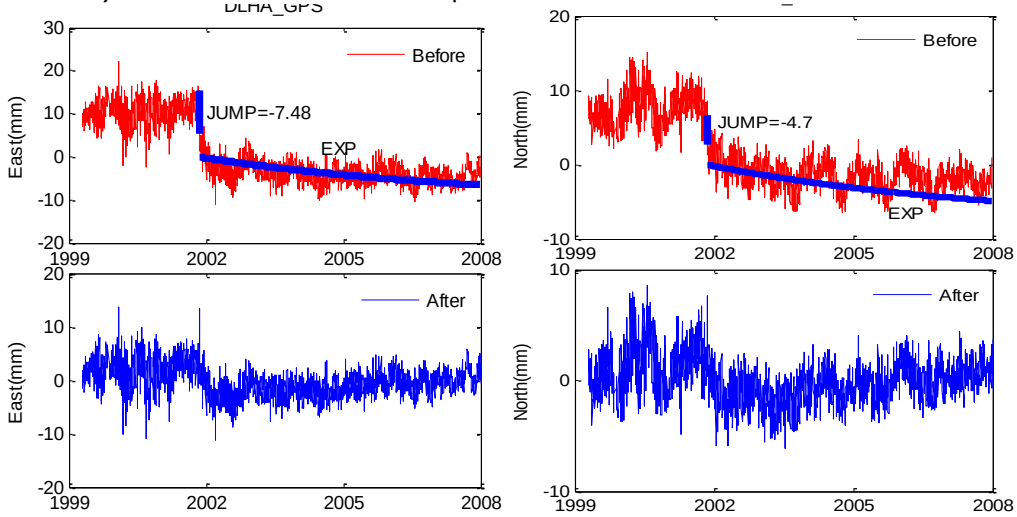

Figure 7 The DLHA time series in east and north component. In the upper subplot, the red points are the original GPS time series, and the vertical blue lines and long solid line are the co-seismic deformation and modeled exponential series separately. The lower subplot shows the coodinates residuals applying an exponential decay function.

The post-seismic slip after the earthquake reveals a clear signature of the viscosity gradient in the crust. We fit the coordinate time series after the 2001 earthquake with an exponential decay function, where the decay time is defined according to Rundle's definitions as $\tau=2*\eta/\mu$ (η, lithosphere viscosity; μ, shear modulus). The result shows the exponential decay function fits nicely (Figure 7). In order to find the effective fitting viscosity for the lithosphere, we test different viscosity value for site DLHA (Table 3). Comparing the derived velocity of observations, we find the optimum viscosity is 4×10^{19} Pa·s and the modeled velocity by post-seismic deformation theory for DLHA are *-0.22 mm yr^{-1}* and *-0.10mm yr^{-1}* for the east and north components.

Table 3 Results of the post-seismic deformation induced by 2001 Kokoxili Earthquakes.

	Viscosity (Pa·s)	Time interval	Velocity at site DLHA	
Modeled from GPS observation		1999.0 – 2008.0	*Ve =-0.19mm yr^{-1}*	*Vn =-0.14mm yr^{-1}*
Modeled by post-seismic deformation theory	1×10^{19}		Ve =-0.65mm yr^{-1}	Vn=-0.33mm yr^{-1}
	2×10^{19}		Ve =-0.44mm yr^{-1}	Vn=--0.19mm yr^{-1}
	3×10^{19}		Ve =-0.29mm yr^{-1}	Vn=-0.13mm yr^{-1}
	4×10^{19}		*Ve =-0.22mm yr^{-1}*	*Vn=-0.10mm yr^{-1}*
	5×10^{19}		Ve =-0.18mm yr^{-1}	Vn=-0.8mm yr^{-1}

Conclusions

We present the latest results from the CMONOC data analysis center at the SHAO. On the basis of

the routine GNSS data analysis of the CMONOC and IGS sites, we present three new achievements: (1) the velocity field of continuous stations, which is released for the first time based on the combination of five years' daily solutions; (2) troposperic zenith delay modeling over China mainland, showing accuracy around 3.5 cm, which is better than other published models; and (3) earthquake co-seismic monitoring and optimum estimation of lithosphere viscosity for the post-seimic deformation modeling.

ACKNOWLEDGMENTS

This paper is supported by the National Natural Science Foundation of China (NSFC) (Grant No. 11673050 and 11273046), the National High Technology Research and Development Program of China (Grant No. 2014AA123102,2013AA122402) and the 100 Talents Programme of The Chinese Academy of Sciences.

REFERENCES

1 Wang Yong, Liu Lintao, Liang Hongyou, Ding Keliang, et al. Research on precipitable water vapor in plateau and plain areas with GPS technique. Journal of Geodesy and Geodynamics, 2006，26(1):88-92 (in Chinese).

2 Liu Jingnan, Shi Chuang, Xu Caijun, Jiang Weiping. Present_day Crustal Movement Speed Field of China Continent Block using Local Repeated GPS Network. Geomatics and Information Science of Wuhan University, 2001,26(3):189-195 (in Chinese).

3 Chen Junping, Wu Bin, Hu Xiaogong, Li Haojun. Shanghai astronomical observatory CMONOC data analysis center.The third China satellite navigation academic conference electronic proceedings-S08 satellite navigation model and method, 2012 (in Chinese).

4 Chen, Junping, Wu, Bin; Hu, Xiaogong; Li, Haojun, SHA: The GNSS analysis center at SHAO. Lecture Notes in Electrical Engineering, v 160 LNEE, p 213-221, 2012, Proceedings - 3rd China Satellite Navigation Conference, CSNC 2012, Revised Selected Papers

5 Shanghai Astronomical Observatory GNSS Analysis Center: www.shao.ac.cn/shao_gnss_ac.

6 Dong, D., Herring, T.A. & King, R.W., 1998. Estimating regional deformation from a combination of space and terrestrial geodetic data, J. Geodyn., 72, 200–214.

7 Dong Danan, Fang Peng, et al. Spatiotemporal filtering using principal component analysis and Karhunen-Loeve expansion approaches for regional GPS network analysis. Journal of Geophysical Research. 2006.111.B03405

8 Wang Min, Shen Zhengkang, Niu Zhijun, et al. The crustal movement of and activity block model. Science in China: 2003.33 (in Chinese).

9 Ye Shuhua, Huang Cheng. Astrogeodynamics. Shandong Science and Technology Press. 2000 (in Chinese).

10 Barnes R A, Leonard R S.Observations of ionospheric disturbance following the Alaska earthquake. J Geophys Res,1965,70(9):1250-1253

11 Zhao Ying, Zhang Xiaohong, Liu Jingnan. The ionospheric electron content disturbance analysis before and after the WenChun earthquake.Progress in geophysics, 2010,25(4):447-453 (in Chinese).

12 Zhang Xiaohong, Guo Bofeng. Real-time tracking the instantaneous movement of crust during earthquake with a stand-alone GPS receiver. Chinese Journal of Geophysics, 2013，56（2）:1928-1936 (in Chinese).

13 Colosimo G, Crespi M, Mazzoni A (2011) Real-time GPS seismology with a stand-alone receiver: a preliminary feasibility demonstration. J Geophys Res 116, B11302. doi:10.1029/2010JB0079